Numerical Simulation of a Stratigraphic Model

Véronique Gervais and Roland Masson
Institut Français du Pétrole 1 et 4 av. de Bois Préau 92852 Rueil Malmaison Cedex, France. email : roland.masson@ifp.fr

Abstract. A multi-lithology diffusive stratigraphic model is considered which simulates at large scales in space and time the infill of sedimentary basins governed by the interaction between tectonics displacements, eustatics variations, sediments supply and sediments transport laws. The model accounts for the mass conservation of each sediment lithology resulting in a mixed parabolic, hyperbolic system of PDEs for the lithology concentrations and the sediments thickness. It also takes into account a limit on the rock alteration velocity modelled as a unilaterality constraint. To obtain a robust, fast and accurate simulation, fully and semi-implicit finite volume discretization schemes are derived for which the existence of stable solutions is proved. Then, the set of nonlinear equations is solved using a Newton algorithm adapted to the unilaterality constraint, and preconditioning strategies are defined for the solution of the linear system at each Newton iteration. They are based on an algebraic approximate decoupling of the sediments thickness and the concentrations variables as well as on a proper preconditioning of each variable. These algorithms are studied and compared in terms of robustness, scalability and efficiency on two real basin test cases.

Keywords: stratigraphic modelling, finite volume method, stability analysis, unilaterality constraint, Newton algorithm, linear iterative solver, block preconditioner, algebraic multigrid

1. Introduction

Many resources such as water, energy (oil, gas), ore, are contained in sedimentary basins, the understanding of which is a major issue to optimize the management of ground natural resources, as well as a challenge in terms of physical and numerical modelling.

To determine the ground rocks properties and geometry, geologists have at their disposal two main types of field data. On the one hand, seismic data record the reflections in the basin of mechanical waves emitted at the ground surface. These signals are processed in order to determine the position of the seismic reflectors, defining the geometry of sediments layers at present time. On the other hand, well-log data are obtained by measuring physical properties such as radioactivity or resistivity within a given well, which are interpreted in terms of sedimentology properties of the sediments crossed by the well.

Using these field data, as well as bibliographical data, sedimentologists are able to build a geological model of the basin describing

its infill scenario by sedimentation/erosion in order to characterize the sedimentary facies of the successive sediments layers, in terms of paleo-bathymetry, depositional environment, composition of the sediments, grain sizes, porosity, ... Such models are a starting point of oil exploration studies.

However, field data are very expensive and local in space or time. A sequential stratigraphic numerical model appears as an efficient tool to test several infill scenarios with a limited amount of data, and to interpolate the data, taking into account the physical processes involved in the formation of sedimentary basins.

We shall consider in the following dynamic slope models which simulate the infill of sedimentary basins at large scales in space and time (tens to hundreds of kilometers, and ten thousand to ten million years) governed basically by the interaction of three main processes : first, the tectonics displacements and eustatics variations defining the available space for sedimentation in the basin (called accommodation), second, the sediments supply either at the boundary of the basin at rivers entries or inside the basin by in situ production of sediments, and third, the sediments transport laws in continental, fluvial, or marine environments.

We consider in this article a sedimentary basin in which sediments are modelled as a mixture of several lithologies $i = 1, \ldots, L$ characterized by different grain size populations. The surficial transport process is a multi-lithology diffusive model introduced in (Rivenaes, 1992) and extended in (Granjeon, 1997), (Granjeon and Joseph, 1999) to take into account carbonate production source terms, and the coupling with the water discharge. The mathematical formalization of this model has been rigorously defined in (Eymard and al, 2004). Basicaly, the model assumes that the fluxes are proportional to the slope of the topography and to a lithology fraction c_i^s of the sediments at the surface of the basin, with depth-dependent and lithology dependent diffusion coefficients. Then, the model accounts for the mass conservation of each lithology in the basin. In order to take into account the dissymmetry between sedimentation and erosion, the limited availability in erodible sediments at the surface of the basin is modelled by a constraint on the erosion rate, as introduced by (Granjeon and Joseph, 1999), which measures the rock alteration velocity or weathering rate. The coupling of this constraint with the conservation equations, defined in (Eymard and al, 2004), uses an additional flux limiter variable and a closure equation which takes the form of a unilaterality constraint.

Most of the parameters of a stratigraphic model, e.g. the diffusion coefficients, the sediments supply, and the tectonics and eustatics vari-

ations, need to be fitted on the seismic and well log data using an inversion procedure involving many simulations with a wide range of parameters. Such a calibration requires a fast and robust computation code in order to carry out efficiently a stratigraphic modelling study.

The objective of this article is to define the numerical methods, ranging from time and space discretization schemes to nonlinear and preconditioned iterative linear solvers of the discrete systems, in order to provide an efficient solution to the multi-lithology stratigraphic model defined in (Granjeon, 1997), (Granjeon and Joseph, 1999), and (Eymard and al, 2004). The fully implicit finite volume discretization introduced in (Eymard and al, 2004) is recalled in section 3.1. It is proved to be unconditionally stable and to preserve the physical bounds of the model such as the positivity of the concentrations and the flux limiter. This scheme is designed to capture accurately the nonlinear transitions between the different transport laws governing the physics of a sedimentary basin.

In order to reduce the nonlinearity of the discrete equations and provide a more robust nonlinear solver, a semi-implicit scheme is also presented in section 3.2, based on a decoupled direct solution of the flux limiter, using a sort of the cells in decreasing topographical order. However, the significant gain obtained in term of nonlinear convergence is balanced by a loss of accuracy of the solution at the transition between constrained continental erosion and marine erosion.

The discrete nonlinear systems are solved using a Newton algorithm described in section 4.1 which is adapted to the unilaterality constraint in the case of the fully implicit scheme. Then, we are left with the solution at each Newton iteration of a non-symmetric, ill conditioned sparse linear system for which a preconditioned iterative linear solver is used.

If there exists many efficient preconditioning methods for scalar PDEs, the preconditioning of systems of PDEs coupling variables of mixed types is still a wide open field of research. The solution proposed in section 4.3 is based on three main ideas: an algebraic decoupling of the sediments thickness, flux limiter and concentrations variables, which is an adaptation to our problem of the strategy used in (Behie and Vinsome, 1982), (Edwards, 1998), (Lacroix and al, 2001) and (Scheichl and al, 2002) for multiphase Darcy flows, a direct solve of the concentrations blocks by one Gauss Seidel sweep with the variables sorted by decreasing topographical order, and an algebraic multigrid preconditioner of the sediments thickness block.

These algorithms will be shown on two real test cases (section 5) to provide an efficient, robust, and scalable simulation code with respect to the size of the mesh and the jumps of the diffusion coefficients.

2. Mathematical model

In this section, the stratigraphic model defined in (Eymard and al, 2004) is recalled and completed to take into account the vertical tectonics displacements. It describes the infill of sedimentary basins, at large scales in space and time, governed by the interaction between the three main processes involved in the evolution of the basin : the change in accommodation space (vertical tectonics displacements, sea level variations), the sediment supply, and the sediments transport in the basin. The vertical compaction of the sediments and the in situ production of sediments, e.g. from coral reefs, will not be described in the following for the sake of conciseness, but all the results presented here extend with minor adaptations.

The model will be first described in the single lithology case in section 2.1, and then extended to several lithologies in section 2.2.

2.1. Single lithology stratigraphic model under maximum erosion rate constraint

Let us denote by $\Omega \subset \mathbb{R}^d$, $d = 1$ or 2, the horizontal extension of the basin (see figure 1-(a)) considered as a fixed domain of boundary $\partial\Omega$, let $\mathbf{n}$ be the unit normal outward vector to $\partial\Omega$ and $T > 0$ be a given time. The single lithology sedimentary basin model describes the evolution of the sediments layer thickness, denoted by h, function of $x \in \Omega$ and time $t \in (0, T)$, given the following data :
- the vertical coordinate $z = H(x, t)$ of the base level of the basin, with time variations due to the tectonics displacements assumed to be only vertical; then, $z = h(x, t) + H(x, t)$, $x \in \Omega$ represents the topography of the basin for each time t.
- the sea level $z = H_m(t)$; in the following, we shall denote by $b(x, t) := H_m(t) - (h + H)(x, t)$ the bathymetry at the surface of the basin for $(x, t) \in \Omega \times (0, T)$.
- the sediment supply at the boundary of the basin.

It is known in landscape morphology that, at large scales in time and space, sediments surficial fluxes proportional to the slope of the topography well describe the evolution of a basin geometry. This leads to the definition of the diffusive flux $\mathbf{f}^d = -k\,\nabla(h + H) = k\nabla b$, with $k > 0$ the diffusion coefficient of the sediments measuring their capability to be transported by gravity. This coefficient is modelled by a nonlinear function of the bathymetry usually taken as :

$$k(b) = \begin{cases} k^m & \text{if } b \geq 0, \\ k^c & \text{otherwise,} \end{cases}$$

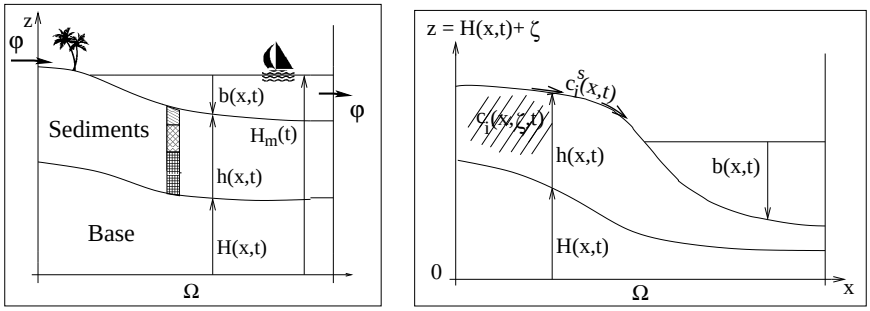

(a) Single lithology case (b) Multi-lithology case

Figure 1. Sedimentary basin

in order to distinguish between the transport of sediments in marine ($b \geq 0$) and continental ($b < 0$) environments. Then, the model accounts for the mass conservation of the sediments, assumed for simplicity to be of constant density and null porosity :

$$\begin{cases} \partial_t h - \Delta\psi(b) = 0 & \text{on } \Omega \times (0,T), \\ -\nabla\psi(b)\cdot\mathbf{n} = \varphi & \text{on } \partial\Omega \times (0,T), \\ h|_{t=0} = h^0 & \text{on } \Omega, \end{cases} \tag{1}$$

with $\psi(b) = -\int_0^b k(u)\,du$, h^0 the initial sediments thickness, and φ the sediments flux at the boundary of the basin.

As explained e.g. in (Anderson and Humphrey, 1989), equation (1) does not take into account the dissymmetry between erosion and sedimentation. Actually, one can distinguish a lower layer composed of non erodible sedimentary rocks and a surficial layer of erodible sediments. This limited availability in erodible sediments is modelled by a constraint on the erosion rate as introduced by (Granjeon and Joseph, 1999) : $\partial_t h \geq -E$ with $E \geq 0$ the maximum erosion rate, measuring the weathering rate or the rock alteration velocity as a function of the bathymetry, climate, humidity, ... In the following, E will be assumed to be a given function of x and t for simplicity.

To couple this constraint with the diffusive model (1), a new variable $\lambda \leq 1$ is introduced to limit the diffusive flux $\mathbf{f}^d$, leading to the definition of the new sediments flux $\mathbf{f} = \lambda\,\mathbf{f}^d$. The closure of the model is obtained by requiring that, if the constraint $\partial_t h > -E$ is satisfied, λ is taken equal to one; and if $\lambda < 1$, the maximum erosion rate is reached : $\partial_t h := -E$. This is the definition of the following unilaterality constraint :

$$\begin{cases} (\partial_t h + E)(1-\lambda) = 0, \\ (\partial_t h + E) \geq 0,\ (1-\lambda) \geq 0 \end{cases} \quad \text{on } \Omega \times (0,T). \tag{2}$$

Let (Γ_e, Γ_s) be a partition of $\partial\Omega \times (0,T)$. An input flux $\varphi_e < 0$ is imposed on Γ_e, but only a maximum output flux $\varphi_s \geq 0$ can be fixed on Γ_s since it may have to be limited, by a unilaterality constraint, to satisfy the constraint on the erosion rate. Finally, the single lithology model is the following :

$$\left\{\begin{array}{rl} \partial_t h + \mathrm{div}\left(-\lambda \nabla \psi(b)\right) = 0 & \text{on } \Omega \times (0,T), \\ (\partial_t h + E)(1-\lambda) = 0 & \text{on } \Omega \times (0,T), \\ (\partial_t h + E) \geq 0,\ (1-\lambda) \geq 0 & \text{on } \Omega \times (0,T), \\ \mathbf{f}\cdot\mathbf{n} = \varphi_e & \text{on } \Gamma_e, \\ (\varphi_s - \mathbf{f}\cdot\mathbf{n})(\partial_t h + E) = 0 & \text{on } \Gamma_s, \\ (\varphi_s - \mathbf{f}\cdot\mathbf{n}) \geq 0,\ (\partial_t h + E) \geq 0 & \text{on } \Gamma_s, \\ h|_{t=0} = h^0 & \text{on } \Omega. \end{array}\right. \tag{3}$$

Let us note that this model can only be well-posed if $\lambda \geq 0$. This stability property for λ will be proved in the discrete case, and the continuous model has been studied in the case of a given diffusive flux $\mathbf{f}^d$ in (Eymard and Gallouët, 2004).

Let us illustrate the model on the example of a progradation of a one-dimensional Delta. In this test case, the base level is constant, the sea level is decreasing, and an input flux is imposed at the left boundary of the basin. Figure 2 exhibits the topography of the basin at successive times for (a) no constraint on the erosion rate, and (b) a maximum erosion rate fixed to 2 m/My. In both cases, one can notice sharp slope discontinuities s at the shorelines due to the jump of the diffusion coefficient. This contrast of the diffusion coefficient is explained by the high transport capacity in continental environment, whereas in marine environment the sediments are retained by the waves. On figure (a), the high transport capacity in continental environment is not limited resulting in a very flat profile. By contrast, on figure (b), the sediments erosion is constrained by the maximum erosion rate which leads to a continental basin profile smoothly following the sea level decrease.

2.2. Extension to the multi-lithology case

The sediments are modelled as a mixture of L lithologies characterized by their grain size population and considered as incompressible materials of constant grain density and null porosity (no compaction).

The basin sediments are described by their L concentrations $c_i \geq 0$ in lithology i defined on the domain $\mathcal{B} = \{(x,\zeta,t)\,|\,(x,t) \in \Omega \times (0,T),\ \zeta \in (-\infty, h(x,t))\}$ (see figure 1-(b)) and satisfying $\sum_{i=1\ldots L} c_i = 1$. The sediments transported at the surface of the basin, i.e. deposited in case of sedimentation or passing through the surface in case of ero-

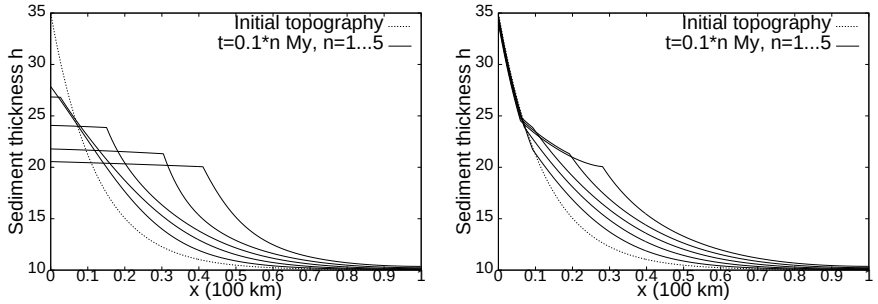

(a) No constraint on the erosion rate

(b) Constraint on the erosion rate (E=2 m/Ma)

Figure 2. Progradation of a Delta : evolution of the sediments thickness h during 0.5 My (a) without constraint on the erosion rate, and (b) with a constraint on the erosion rate ($E = 2$ m/My). The diffusion coefficient k is taken equal to $5.10^4\ m^2/y$ in continental environment and $10^3\ m^2/y$ in marine environment.

sion, are described by their L surface concentrations $c_i^s \geq 0$ defined on $\Omega \times (0,T)$ and also verifying $\sum_{i=1\ldots L} c_i^s = 1$.

Since the compaction is not considered, and since the sediments transport only occurs at the surface of the basin, the composition inside the basin remains constant : $\partial_t c_i = 0$ on $\mathcal{B}$. The evolution of c_i is only governed by the boundary condition at the top of the basin stating that $c_i|_{\zeta=h} = c_i^s$ in case of sedimentation ($\partial_t h > 0$). This yields

$$\left\{ \begin{array}{rl} \partial_t c_i = 0 & \text{on } \mathcal{B}, \\ c_i|_{\zeta=h} = c_i^s & \text{on } \{(x,t) \in \Omega \times (0,T) \,|\, \partial_t h(x,t) > 0\}, \\ c_i|_{t=0} = c_i^0 & \text{on } \{(x,\zeta) \,|\, x \in \Omega,\ \zeta \in (-\infty, h|_{t=0}(x))\}, \end{array} \right.$$

where c_i^0, $i = 1, \ldots, L$ are the initial concentrations in the basin.

These linear hyperbolic equations are coupled to the conservation equations of each lithology on the domain $\Omega \times (0,T)$ accounting for the conservation of the lithology fraction $h_i(x,t) = \int_0^{h(x,t)} c_i(x,\zeta,t)\, d\zeta$: $\partial_t h_i + \operatorname{div} \mathbf{f}_i = 0$ on $\Omega \times (0,T)$ with $\partial_t h_i = c_i|_{\zeta=h}\, \partial_t h$ since $\partial_t c_i = 0$ on $\mathcal{B}$.

The surficial transport model considered here is the multi-lithology diffusive model introduced in (Rivenaes, 1992) for which the flux in lithology i is taken proportional to the surface concentration c_i^s with a diffusion coefficient depending on the lithology i. Hence, the flux in lithology i is given by $\mathbf{f}_i = -c_i^s\ \lambda\ \nabla \psi_i(b)$ with $\psi_i(b) = -\int_0^b k_i(u)\, du$, where $k_i(b)$ is usually modelled by a discontinuous function of the bathymetry as in the single lithology case.

The boundary conditions are set by a maximum total output flux φ_s prescribed on Γ_s, and an input flux φ_e on Γ_e together with the

fractions $\mu_{e,i} \in [0,1]$, $i = 1, \ldots, L$, such that $\sum_{i=1\ldots L} \mu_{e,i} = 1$. In the following, we shall denote by $\varphi_{e,i} = \mu_{e,i}\, \varphi_e$ the input fluxes on Γ_e for all $i = 1, \ldots, L$.

Finally, the multi-lithology diffusive model under maximum erosion rate constraint is the following: for all $i = 1, \ldots, L$

$$\text{Surface: } \left\{ \begin{array}{rll} c_i|_{\zeta=h} \partial_t h + \mathrm{div}\left(-c_i^s\ \lambda \nabla \psi_i(b)\right) &= 0 & \text{on } \Omega \times (0,T), \\ \sum_{j=1}^L c_j^s &= 1 & \text{on } \Omega \times (0,T), \\ (\partial_t h + E)(1-\lambda) &= 0 & \text{on } \Omega \times (0,T), \\ (\partial_t h + E) \geq 0,\ (1-\lambda) &\geq 0 & \text{on } \Omega \times (0,T), \\ \mathbf{f}_i \cdot \mathbf{n} &= \varphi_{e,i} & \text{on } \Gamma_e, \\ (\varphi_s - \sum_{j=1}^L \mathbf{f}_j \cdot \mathbf{n})(\partial_t h + E) &= 0 & \text{on } \Gamma_s, \\ (\varphi_s - \sum_{j=1}^L \mathbf{f}_j \cdot \mathbf{n}) \geq 0,\ (\partial_t h + E) &\geq 0 & \text{on } \Gamma_s, \\ h|_{t=0} &= h^0 & \text{on } \Omega. \end{array} \right. \quad (4)$$

$$\text{Basin: } \left\{ \begin{array}{rl} \partial_t c_i &= 0 \quad \text{on } \mathcal{B}, \\ c_i|_{\zeta=h} &= c_i^s \quad \text{on } \{(x,t) \in \Omega \times (0,T) \,|\, \partial_t h(x,t) > 0\}, \\ c_i|_{t=0} &= c_i^0 \quad \text{on } \{(x,\zeta) \,|\, x \in \Omega,\ \zeta \in (-\infty, h|_{t=0}(x))\}. \end{array} \right. \quad (5)$$

In the case of equal diffusion coefficients for all the lithologies and no constraint on the erosion rate, the existence of a unique weak solution has been proved for this system of PDEs (see (Eymard and al, 2004b) and (Gervais and Masson, 2004)).

3. Finite volume discretization schemes

Our aim is to define a finite volume discretization scheme for the stratigraphic model (4)-(5) that should preserve the physical bounds of the model (stability properties), and capture the nonlinear transitions between the different sediments transport laws within the basin (continental diffusion/marine diffusion, unconstrained erosion/constrained erosion, sedimentation/erosion).

To get such a discretization scheme, the particularities of the model have to be taken into account such as the accumulation term $c_i|_{\zeta=h}\, \partial_t h$ in which the surface concentration only appears in case of sedimentation, the unilaterality constraint, and the sharp jumps of the diffusion coefficients $k_i(b)$ at the shoreline.

An implicit time integration of the sediments thickness is necessary to get an unconditionally stable time discretization scheme. In order to reduce the nonlinearity of the discrete system, one could compute the diffusion coefficients $k_i(b)$ using the bathymetry at the previous time step. However, due to the large jumps of the diffusion coefficients at the shoreline, such a discretization requires very small time steps

to accurately solve the position of the shoreline. In order to capture correctly this position, we shall rather use a time discretization of $\nabla\psi_i(b)$ with $\psi_i(b)$ taken implicit.

The flux limiter λ is approximated using a cell centered variable with an upstream evaluation at the edge between two neighboring cells. Thanks to this upwinding, an approximation of the variable λ can be computed explicitly by induction over the cells sorted by decreasing topographical order for a given approximation of the surface concentrations and sediments thickness variables (Proposition 1). This leads to the definition of a semi-implicit unconditionally stable scheme, decoupling the computation of (h, c_i^s) on the one hand, and λ on the other hand. This scheme is robust but can lack accuracy since the constraint $\partial_t h \geq -E$ is not necessarily satisfied. Alternatively, an implicit integration of λ is unconditionally stable and satisfies the physical bounds thanks to the upstream evaluation (see section 3.1). It is more accurate than the semi-implicit scheme, but the Newton algorithm used to solve the discrete nonlinear system can lack robustness, especially on fine grids (see section 4).

Since there is no time derivative of the surface concentrations c_i^s, this variable has to be discretized implicitly. A decoupling of the (h, λ) variables and the c_i^s variable can be implemented defining an equation for the mixture of lithologies to compute (h, λ). However, depending on the definition of the mixture equation, such schemes will be either unstable when refining the time step, or will not preserve the mass conservation of the lithologies. Hence it will not be retained (see (Gervais, 2004) for details). An implicit time integration of the surface concentrations with an upstream evaluation at the edge between two neighboring cells leads to an unconditionally stable discretization scheme satisfying the physical bounds.

The fully implicit scheme and the semi-implicit scheme will be presented in sections 3.1 and 3.2 respectively, as well as existence and stability results for the solutions.

3.1. Fully implicit discretization scheme

This scheme uses a cell-centered finite volume method in space and an implicit time integration of all the variables h, λ and c_i^s, $i = 1, \ldots, L$. It has already been introduced in (Eymard and al, 2004) and will be briefly recalled in section 3.1.1. In paragraph 3.1.2, the existence of a stable solution for this scheme will be proved and stability results will be obtained in section 3.1.3.

3.1.1. *Finite volume scheme*
In the sequel, we shall consider admissible finite volume meshes of the domain Ω according to the following definition, introduced in (Eymard and al, 2000). They will be denoted by $(\mathcal{K}, \Sigma_{int}, \mathcal{P})$.

*Definition 1. (*Admissible meshes*)* Let $\mathcal{K}$ be the set of open control volumes of Ω, let $\mathcal{P} = (x_\kappa)_{\kappa\in\mathcal{K}}$ be a family of points of Ω such that $x_\kappa \in \bar{\kappa}$, and let Σ_{int} be the set of interior edges σ of the mesh such that there exist $\kappa, \kappa' \in \mathcal{K}$, $\kappa \neq \kappa'$, with $m(\bar{\kappa} \cap \bar{\kappa}') > 0$, $\sigma = \bar{\kappa} \cap \bar{\kappa}'$ (denoted by $\kappa|\kappa'$), and m the Lebesgue measure of dimension $d-1$. The triplet $(\mathcal{K}, \Sigma_{int}, \mathcal{P})$ defines an admissible mesh iff the following properties are satisfied :
(i) $\bigcup_{\kappa\in\mathcal{K}} \bar{\kappa} = \bar{\Omega}$,
(ii) each interior edge $\sigma \in \Sigma_{int}$ is included in an hyperplane of $\mathbb{R}^d$,
(iii) for each interior edge $\sigma = \kappa|\kappa'$, one has $x_\kappa \neq x_{\kappa'}$ and the line $x_\kappa x_{\kappa'}$ is orthogonal to σ,
(iv) for all $\kappa \in \mathcal{K}$, there exists a subset Σ_κ of Σ_{int} such that $\partial\kappa \setminus \partial\Omega = \bar{\kappa} \setminus (\kappa \cup \partial\Omega) = \cup_{\sigma\in\Sigma_\kappa} \bar{\sigma}$.

In the sequel, $|\kappa|$ (resp. $|\sigma|$) is the d-dimensional measure $m(\kappa)$ of the cell κ (resp. the $(d-1)$-dimensional measure $m(\sigma)$ of the edge $\sigma \in \Sigma_{int}$), $\mathcal{K}_\kappa$ the set of neighboring cells of κ (excluding κ), $T_{\kappa\kappa'} = T_\sigma$ the transmissibility of the edge $\sigma = \kappa|\kappa'$, defined by $T_{\kappa\kappa'} := \frac{|\sigma|}{d(\kappa,\kappa')}$ with $d(\kappa, \kappa')$ the distance between the points x_κ and $x_{\kappa'}$, and $\mathbf{n}_{\kappa\kappa'}$ the unit normal vector to $\sigma = \kappa|\kappa'$ outward to κ. We shall also denote by $X(\mathcal{K})$ the set of real valued functions on Ω which are constant over each control volume of the mesh.

The time discretization is denoted by $t^n, n \in \mathbb{N}$, such that $t^0 = 0$ and $\Delta t^{n+1} = t^{n+1} - t^n > 0$. In the following, the superscript n, $n \in \mathbb{N}$, will be used to denote that the variables are considered at time t^n.

The fully implicit discretization of (4)-(5) has already been introduced in (Eymard and al, 2004). Let us just highlight two of its main characteristics. First, the conservation equations (4) are integrated over $\kappa \times (t^n, t^{n+1})$, and the fluxes at the edges of the control volume κ are approximated using all variables at time t^{n+1} and an upstream evaluation of the surface concentrations and the flux limiter λ. This choice leads to the stability of the scheme (see Proposition 3). Second, the approximation of the concentration c_i in the basin is, for each cell

κ, the solution at time t^{n+1} of :

$$\left\{\begin{array}{rl} \partial_t c_{i,\kappa}(\zeta,t) = 0 & \text{for all } t \in (t^n, t^{n+1}),\ \zeta \in (-\infty, h_\kappa(t)), \\ c_{i,\kappa}(h_\kappa(t),t) = c_{i,\kappa}^{s,n+1} & \text{if } h_\kappa^{n+1} > h_\kappa^n, \\ c_{i,\kappa}(\zeta,t^n) = c_{i,\kappa}^n(\zeta) & \text{for all } \zeta \in (-\infty, h_\kappa^n), \end{array}\right.$$

with $h_\kappa(t) = h_\kappa^n + (t-t^n)(h_\kappa^{n+1} - h_\kappa^n)/\Delta t^{n+1}$, and the discretization of the accumulation term in (4) is taken equal to

$$\Delta h_{i,\kappa}^{n+1} = \int_0^{h_\kappa^{n+1}} c_{i,\kappa}^{n+1}(\zeta)\, d\zeta - \int_0^{h_\kappa^n} c_{i,\kappa}^n(\zeta)\, d\zeta.$$

For all control volumes $\kappa \in \mathcal{K}$, the following initial values are defined:

1. h_κ^0 is the initial approximation of h in κ,
2. $c_{i,\kappa}^0(\zeta)$, for all species i, is the approximation of c_i^0 on the cell κ, defined for $\zeta \in (-\infty, h_\kappa^0)$, non negative and satisfying $\sum_{i=1}^L c_{i,\kappa}^0 = 1$.

The discretization of equations (4)-(5) within a given control volume $\kappa \in \mathcal{K}$ between times t^n and t^{n+1} is given by :

Conservation of surface sediments:

$$\begin{array}{c} \dfrac{\Delta h_{i,\kappa}^{n+1}}{\Delta t^{n+1}}\,|\kappa| \;+\; \displaystyle\sum_{\kappa' \in \mathcal{K}_\kappa} T_{\kappa\kappa'} \lambda_{\kappa\kappa'}^{n+1} c_{i,\kappa\kappa'}^{s,n+1} [\psi_i(b_\kappa^{n+1}) - \psi_i(b_{\kappa'}^{n+1})] \;+ \\ \varphi_{\kappa,e,i}^{n+1} \;+\; \lambda_\kappa^{n+1} \mu_{i,\kappa}^{n+1} \varphi_{\kappa,s}^{n+1} = 0, \end{array} \tag{6}$$

$$\sum_{i=1}^L c_{i,\kappa}^{s,n+1} = 1, \tag{7}$$

Conservation of basin sediments:

$$\text{if } h_\kappa^{n+1} \geq h_\kappa^n \quad \left\{\begin{array}{l} \Delta h_{i,\kappa}^{n+1} = c_{i,\kappa}^{s,n+1}(h_\kappa^{n+1} - h_\kappa^n), \\ c_{i,\kappa}^{n+1}(\zeta) = c_{i,\kappa}^n(\zeta) \text{ for all } \zeta \in (-\infty, h_\kappa^n), \\ c_{i,\kappa}^{n+1}(\zeta) = c_{i,\kappa}^{s,n+1} \text{ for all } \zeta \in (h_\kappa^n, h_\kappa^{n+1}), \end{array}\right. \tag{8}$$

$$\text{otherwise} \quad \left\{\begin{array}{l} \Delta h_{i,\kappa}^{n+1} = \int_{h_\kappa^n}^{h_\kappa^{n+1}} c_{i,\kappa}^n(\zeta)\, d\zeta, \\ c_{i,\kappa}^{n+1}(\zeta) = c_{i,\kappa}^n(\zeta) \text{ for all } \zeta \in (-\infty, h_\kappa^{n+1}), \end{array}\right. \tag{9}$$

Constraint:

$$\left\{\begin{array}{c} (h_\kappa^{n+1} - \mathcal{H}_\kappa^{n+1})(1 - \lambda_\kappa^{n+1}) = 0, \\ (h_\kappa^{n+1} - \mathcal{H}_\kappa^{n+1}) \geq 0,\ (1 - \lambda_\kappa^{n+1}) \geq 0. \end{array}\right. \tag{10}$$

In (6)-(10), the following notations are used.

1. h_κ^{n+1} (resp. λ_κ^{n+1}, $c_{i,\kappa}^{s,n+1}$) is the approximation of the sediments thickness h (resp. the flux limiter λ, the surface sediments concentration c_i^s in lithology i) at time t^{n+1} in κ;

2. the function $c^n_{i,\kappa}$, defined for $\zeta \in (-\infty, h^n_\kappa)$, is the approximation of the sediments concentration in lithology i in the column $\{(x,\zeta)|x \in \kappa, \zeta \in (-\infty, h(x,t^n))\}$ at time t^n;

3. b^n_κ is the approximation of the bathymetry at time t^n in κ, defined by $b^n_\kappa := H_m(t^n) - (h^n_\kappa + H_\kappa(t^n))$ with $H_\kappa(t)$ the approximation of H at time t on κ;

4. $c^{s,n+1}_{i,\kappa\kappa'}$ (resp. $\lambda^{n+1}_{\kappa\kappa'}$) is the upstream weighted evaluation of the surface sediments concentration in lithology i (resp. the flux limiter) at the edge σ between the cells κ and κ' with respect to the sign of $\nabla\psi_i \cdot \mathbf{n}_{\kappa\kappa'}$:

$$c^{s,n+1}_{i,\kappa\kappa'} = \begin{cases} c^{s,n+1}_{i,\kappa} \text{ if } \psi_i(b^{n+1}_\kappa) > \psi_i(b^{n+1}_{\kappa'}), \\ c^{s,n+1}_{i,\kappa'} \text{ otherwise }, \end{cases}$$

$$\lambda^{n+1}_{\kappa\kappa'} = \begin{cases} \lambda^{n+1}_{\kappa} \text{ if } \psi_i(b^{n+1}_\kappa) > \psi_i(b^{n+1}_{\kappa'}), \\ \lambda^{n+1}_{\kappa'} \text{ otherwise }. \end{cases}$$

   Let us point out that this upwinding is independent of the lithology and only depends on the topography.

5. $\varphi^{n+1}_{\kappa,e,i}$ and $\varphi^{n+1}_{\kappa,s}$ are approximations of the input flux in lithology i and the global output flux at the boundary of the cell κ, defined by:

$$\varphi^{n+1}_{\kappa,e,i} = \int_{\partial\kappa\times(t^n,t^{n+1})\cap\Gamma_e} \varphi_{e,i}\, d\sigma\, dt, \;\; \varphi^{n+1}_{\kappa,s} = \int_{\partial\kappa\times(t^n,t^{n+1})\cap\Gamma_s} \varphi_s\, d\sigma\, dt.$$

6. $\mathcal{H}^{n+1}_\kappa$ is the exact solution at time t^{n+1} of the ordinary differential equation

$$\begin{cases} \frac{d\mathcal{H}}{dt} = -E_\kappa(t), \\ \mathcal{H}(t^n) = h^n_\kappa, \end{cases}$$

   with $E_\kappa(t) = \frac{1}{|\kappa|}\int_\kappa E(x,t)\,dx$ supposed to be of class C^1; $\mathcal{H}^{n+1}_\kappa$ also satisfies $E^{n+1}_\kappa := \frac{h^n_\kappa - \mathcal{H}^{n+1}_\kappa}{\Delta t^{n+1}} \geq 0$ and the constraint on the erosion rate rewrites as $h^{n+1}_\kappa \geq \mathcal{H}^{n+1}_\kappa$;

7. $\mu^{s,n+1}_{i,\kappa}$ is the fractional flow $\dfrac{c^{s,n+1}_{i,\kappa}\psi_i'(b^{n+1}_\kappa)}{\sum_{j=1}^L c^{s,n+1}_{j,\kappa}\psi_j'(b^{n+1}_\kappa)}$.

Let us note that, to obtain a fully discrete scheme, the initial condition $c^0_{i,\kappa}(\zeta)$ is projected on a piecewise constant mesh for each κ in the direction ζ. Then, the scheme (6)–(10) generates a piecewise

constant approximation of $c_{i,\kappa}^n(\zeta)$ on each cell κ for all $i = 1, \ldots, L$, with time-dependent mesh sizes in the direction ζ.

In the discretization scheme (6)–(10), the solution of the discrete concentrations $c_{i,\kappa}^{n+1}$ is explicit and decoupled from the computation of the other variables. Thus, we are left at each time step with the solution of a nonlinear system of $(L+2) \times \#\mathcal{K}$ unknowns, i.e. the discrete variables h_κ^{n+1}, λ_κ^{n+1} and $c_{i,\kappa}^{s,n+1}$ on each cell $\kappa \in \mathcal{K}$ for all the lithologies $i = 1, \ldots, L$. In the sequel, we shall prove the existence of stable solutions for this problem (sections 3.1.2 and 3.1.3).

For the sake of simplicity, it is assumed in the remaining of this section that $\Delta t = \Delta t^n$ for all $n \geq 1$, although the results presented readily extend to variable time steps. For a given time $T > 0$, let $N_{\Delta t}$ denote the integer such that $t^{N_{\Delta t}} < T \leq t^{N_{\Delta t}+1}$.

The convergence of this scheme towards a weak solution has been proved in (Eymard and al, 2004b) in the case of unitary diffusion coefficients without constraint on the erosion rate.

3.1.2. *Existence of stable solutions*

In this section, we shall prove the existence of stable solutions, stated in Proposition 2, for the system (6)–(10). The proof uses the Brouwer fixed point theorem (given in (Kavian, 1993) for example) and an explicit computation of the flux limiter for a given approximation of the sediments thickness and surface concentrations variables stated in Proposition 1.

Let sediments thicknesses $(h_\kappa^{n+1})_{\kappa\in\mathcal{K}}$ and non negative surface concentrations $(c_{i,\kappa}^{s,n+1})_{\kappa\in\mathcal{K},\, i=1,\ldots,L}$ be given. Using the sum over the lithologies of the conservation equations (6) and equation (7), one can rewrite the sedimentation rate as

$$\begin{aligned}\frac{h_\kappa^{n+1} - h_\kappa^n}{\Delta t^{n+1}} |\kappa| = &- \sum_{i=1}^{L} \sum_{\kappa' \in \mathcal{K}_\kappa} T_{\kappa\kappa'} \lambda_{\kappa\kappa'}^{n+1} c_{i,\kappa\kappa'}^{s,n+1} [\psi_i(b_\kappa^{n+1}) - \psi_i(b_{\kappa'}^{n+1})] \\ &- \lambda_\kappa^{n+1} \varphi_{\kappa,s}^{n+1} - \sum_{i=1}^{L} \varphi_{\kappa,e,i}^{n+1}.\end{aligned} \tag{11}$$

Proposition 1. The solution $(\lambda_\kappa^{n+1})_{\kappa\in\mathcal{K}}$ of the discrete unilaterality constraint (10) for which the sedimentation rate is given by (11) can be computed explicitly by induction over the control volumes sorted by decreasing topographical order : it is given by

$$\begin{cases} \lambda_\kappa^{n+1} = \min\left(1, \frac{\alpha_\kappa^{n+1}}{\beta_\kappa^{n+1}}\right) & \text{if } \beta_\kappa^{n+1} > 0, \\ \lambda_\kappa^{n+1} = 1 & \text{if } \beta_\kappa^{n+1} = 0, \end{cases} \tag{12}$$

with

$$\begin{aligned}\alpha_\kappa^{n+1} &= |\kappa| E_\kappa^{n+1} - \sum_{i=1}^{L} \varphi_{\kappa,e,i}^{n+1} \\ &\quad + \sum_{\substack{\kappa' \in \mathcal{K}_\kappa, \\ b_\kappa^{n+1} \geq b_{\kappa'}^{n+1}}} T_{\kappa\kappa'} \lambda_{\kappa'}^{n+1} \Big[\sum_{i=1}^{L} c_{i,\kappa'}^{s,n+1} [\psi_i(b_{\kappa'}^{n+1}) - \psi_i(b_\kappa^{n+1})] \Big], \\ \beta_\kappa^{n+1} &= \sum_{\substack{\kappa' \in \mathcal{K}_\kappa, \\ b_\kappa^{n+1} < b_{\kappa'}^{n+1}}} T_{\kappa\kappa'} \Big[\sum_{i=1}^{L} c_{i,\kappa}^{s,n+1} [\psi_i(b_\kappa^{n+1}) - \psi_i(b_{\kappa'}^{n+1})] \Big] + \varphi_{\kappa,s}^{n+1},\end{aligned} \tag{13}$$

and satisfies $\lambda_\kappa^{n+1} \in [0,1]$ for all $\kappa \in \mathcal{K}$.

Let us point out that, for a cell κ such that $\alpha_\kappa^{n+1} = \beta_\kappa^{n+1} = 0$, the solution λ_κ^{n+1} is arbitrary such that $\lambda_\kappa^{n+1} \leq 1$ (arbitrarily fixed to one in (12)), but the fluxes at the edges of the cells are in any case defined in an unequivocal way.

The existence of a solution to the system (6)–(10) satisfying the physical bounds for the flux limiter and the concentrations is stated in the following proposition. The proof uses the Brouwer fixed point theorem on a function defined using (12) having the solution of (6)–(10) as fixed point (see (Gervais, 2004) for further details).

Proposition 2. Let us assume that, for all $t \geq 0$ and $i = 1, \ldots, L$, $H(.,t) \in L^\infty(\Omega)$, and $\varphi_{e,i},\ \varphi_s \in L^\infty(\partial\Omega \times \mathbb{R}_+^*)$. Let $T > 0$, $\Delta t > 0$ and $(\mathcal{K}, \Sigma_{int}, \mathcal{P})$ be an admissible mesh of Ω in the sense of Definition 1. Then, for all $n \in \{0, \ldots, N_{\Delta t}\}$, there exists at least a solution $(h_\kappa^{n+1}, \lambda_\kappa^{n+1}, c_{1,\kappa}^{s,n+1}, \ldots, c_{L,\kappa}^{s,n+1})_{\kappa\in\mathcal{K}}$ and $(c_{1,\kappa}^{n+1}, \ldots, c_{L,\kappa}^{n+1})_{\kappa\in\mathcal{K}}$ to the set of equations (6)–(10) which satisfies, for all $\kappa \in \mathcal{K}$, $n \in \mathbb{N}$ and $i = 1, \ldots, L$,

$$\begin{cases} \lambda_\kappa^{n+1} \geq 0, \\ c_{i,\kappa}^{s,n+1} \in [0,1], \\ c_{i,\kappa}^{n+1}(\zeta) \in [0,1] \quad \text{for all } \zeta \in (-\infty, h_\kappa^{n+1}). \end{cases} \tag{14}$$

3.1.3. *Stability results*

In this section, we will prove some stability results for the discrete variables. Proposition 2 states the existence of at least one solution for problem (6)–(10) satisfying the physical bounds for λ and the concentrations. Under some additional assumptions, satisfied in usual simulations, one can prove that any solution verifies these bounds. This result is stated in Proposition 3 and has already been proved in (Eymard and al, 2004). Proposition 4 states a stability result for the sediments thickness.

Proposition 3. Let us assume that either $k_i(b) = k(b)$ for all $i = 1, \ldots, L$, or $\varphi_s = 0$ on Γ_s. Let $(\mathcal{K}, \Sigma_{int}, \mathcal{P})$ be an admissible mesh of Ω in the sense of Definition 1. Then any solution of (6)–(10) satisfies, for all $\kappa \in \mathcal{K}$ and $n \in \mathbb{N}$,

$$\begin{array}{l} \lambda_\kappa^{n+1} \geq 0, \\ c_{i,\kappa}^{s,n+1} \in [0,1] \ \forall\, i = 1, \ldots, L, \end{array}$$

except for the singular points $(\kappa, n+1)$ defined below. Furthermore,

$$c_{i,\kappa}^{n+1}(\zeta) \in [0,1] \quad \forall\, n \in \mathbb{N},\ \kappa \in \mathcal{K},\ i = 1, \ldots, L \text{ and } \zeta \in (-\infty, h_\kappa^{n+1}).$$

The singular points $(\kappa, n+1)$ are the ones for which the fluxes at the edges of the control volume κ vanish and $h_\kappa^{n+1} = h_\kappa^n$. In such cases, the concentrations $c_{i,\kappa}^{s,n+1}$, $i = 1, \ldots, L$, can be chosen arbitrarily such that their sum over the species i is equal to one. If $E_\kappa^{n+1} > 0$, the flux limiter λ_κ^{n+1} is equal to one; and if $E_\kappa^{n+1} = 0$, it vanishes (for $\beta_\kappa^{n+1} = 0$), or is arbitrary in the interval $(-\infty, 1]$ (for $\beta_\kappa^{n+1} > 0$).

In the case of homogeneous Neumann boundary conditions, the stability of the approximate sediments thickness in $L^\infty(0,T;L^2(\Omega))$ norm is stated in Proposition 4. The proof, given in (Gervais, 2004), starts from the sum over i of the surface conservation equations (6) and uses the positivity of the discrete concentrations and flux limiter, Young's inequality and the Gronwall Lemma (given in (Heywood and Rannacker, 1990) for example).

Proposition 4. Let us assume that $H \in L^2(\mathbb{R}_+; H^1(\Omega))$, $h^0 \in L^2(\Omega)$, $\varphi_e = \varphi_s = 0$ on $\partial\Omega \times \mathbb{R}_+^*$. Let $T > 0$, $(\mathcal{K}, \Sigma_{int}, \mathcal{P})$ be an admissible mesh of Ω in the sense of Definition 1, and $(h_\kappa^{p+1})_{\kappa \in \mathcal{K},\, p \in \{0,\ldots,N_{\Delta t}\}}$ be a solution of (6)–(10). For all $n \in \{0, \ldots, N_{\Delta t}\}$, let us define $h_{\mathcal{K}}^{n+1} \in X(\mathcal{K})$ by $h_{\mathcal{K}}^{n+1}(x) = h_\kappa^{n+1}$ for all $x \in \kappa$, $\kappa \in \mathcal{K}$. Then, there exists $C_1 > 0$ only depending on Ω, T, h^0, H, and $k_i(b)$, $i = 1, \ldots, L$, such that $||h_{\mathcal{K}}^{n+1}||_{L^2(\Omega)} \leq C_1$ for all $n \in \{0, \ldots, N_{\Delta t}\}$.

3.2. Semi-implicit scheme: decoupling of the flux limiter variable

Let us now define the semi-implicit finite volume scheme for which the solution of the flux limiter variable λ is decoupled at each time step from the computation of the other unknowns. This scheme uses the property stated in Proposition 1.

Using the same notations as in the previous section, let us consider the finite volume discretization scheme defined on each control volume $\kappa \in \mathcal{K}$ between times t^n and t^{n+1} by

$$\frac{\Delta h_{i,\kappa}^{n+1}}{\Delta t^{n+1}}|\kappa| + \sum_{\kappa' \in \mathcal{K}_\kappa} T_{\kappa\kappa'} \lambda_{\kappa\kappa'}^{n,n+1} c_{i,\kappa\kappa'}^{s,n+1} [\psi_i(b_\kappa^{n+1}) - \psi_i(b_{\kappa'}^{n+1})] + \varphi_{\kappa,e,i}^{n+1} + \lambda_\kappa^n \mu_{i,\kappa}^{n+1} \varphi_{\kappa,s}^{n+1} = 0, \tag{15}$$

$$\text{with } \lambda_{\kappa\kappa'}^{n,n+1} = \begin{cases} \lambda_\kappa^n & \text{if } h_\kappa^{n+1} + H_\kappa^{n+1} \geq h_{\kappa'}^{n+1} + H_{\kappa'}^{n+1}, \\ \lambda_{\kappa'}^n & \text{if } h_\kappa^{n+1} + H_\kappa^{n+1} < h_{\kappa'}^{n+1} + H_{\kappa'}^{n+1}, \end{cases}$$

together with equations (7)–(9), and the flux limiter λ_κ^{n+1} given by (12). At the first time step, the flux limiter λ_κ^0 is computed by (12) using the initial sediments thickness and an initialization of the surface concentrations that can be roughly derived from the input fluxes and the basin initial concentrations. It results that the semi-implicit scheme should be preferably initialized using a small initial time step or the solution of the fully implicit scheme at the first time step.

The computation of the unknowns $c_{i,\kappa}^{n+1}$ and λ_κ^{n+1}, $\kappa \in \mathcal{K}$, $i = 1, \ldots, L$, is explicit and decoupled from the other variables. The concentrations are determined using (8)-(9) and the flux limiters are computed by induction over the cells sorted by decreasing topographical order using (12). At each time step, we are left with the solution of a nonlinear system of size $(L+1) \times \#\mathcal{K}$ for the discrete variables h_κ^{n+1} and $c_{i,\kappa}^{s,n+1}$ on each cell $\kappa \in \mathcal{K}$ for all the lithologies $i = 1, \ldots, L$.

The existence of solutions for the fully implicit scheme (6)–(10) stated in Proposition 2 readily extends to the semi-implicit scheme (15),(7)-(9),(12). The stability property stated in Proposition 4 for the sediments thickness variable is also valid, as well as the one stated in Proposition 3 for the concentrations and the flux limiter variables (with the positivity of λ given by Proposition 1).

Finally, let us point out that the solutions of the semi-implicit scheme do not necessarily satisfy the constraint $h_\kappa^{n+1} \geq \mathcal{H}_\kappa^{n+1}$.

4. Linear and nonlinear solvers

4.1. Newton algorithm

The fully implicit scheme (6)–(10) is solved at each time step using a Newton algorithm adapted to the unilaterality constraint introduced in (Eymard and al, 2000) for the black-oil two phase Darcy flow model.

Let $\mathcal{I} = (\mathcal{I}_\kappa)_{\kappa \in \mathcal{K}} \in \{0,1\}^{\#\mathcal{K}}$ be a binary phase index where $\mathcal{I}_\kappa = 0$ corresponds to the diffusive transport ($\lambda_\kappa := 1$, $h_\kappa \geq \mathcal{H}_\kappa$) and $\mathcal{I}_\kappa = 1$ to the weather limited transport ($\lambda_\kappa < 1$, $h_\kappa := \mathcal{H}_\kappa$). Then, a Newton

iteration is applied to the set of nonlinear equations (6), $i = 1, \ldots, L$, considered as functions of the variables $c^s = (c^s_{i,\kappa})_{i=1,\ldots,L,\, i\neq e,\, \kappa\in\mathcal{K}}$ and a variable $y = (y_\kappa)_{\kappa\in\mathcal{K}}$ defined by

$$y_\kappa = \begin{cases} h_\kappa & \text{if } \mathcal{I}_\kappa = 0 \ (\lambda_\kappa = 1), \\ \lambda_\kappa & \text{if } \mathcal{I}_\kappa = 1 \ (h_\kappa = \mathcal{H}_\kappa), \end{cases} \tag{16}$$

to compute the steps δc^s and δy. This definition of the y variable guarantees at each iteration that the product $(1-\lambda_\kappa)(h_\kappa - \mathcal{H}_\kappa)$ vanishes. Once the variables c^s and y have been incremented, the phase index $\mathcal{I}$ is updated in order to satisfy the inequality constraints $1-\lambda_\kappa \geq 0$ and $h_\kappa \geq \mathcal{H}_\kappa$, and the algorithm is iterated until sufficient reduction of the residuals of equations (6).

The concentrations $c^{s,n+1}_{e,\kappa}$ have been eliminated using equation (7). In the sequel, the subscript e will be taken equal to 1 to fix ideas. The choice of e does not change the Newton convergence but will be crucial for the efficiency of the linear solver presented in section 4.3. It will be discussed in paragraph 5.

Finally, if the solution satisfies $\lambda_\kappa \geq 0$ and $c^s_{i,\kappa} \in [0,1]$ for all $i = 1, \ldots, L$ and $\kappa \in \mathcal{K}$ at convergence (Proposition 3), this is not necessarily the case of the Newton iterates and these constraints are therefore imposed : for all $\kappa \in \mathcal{K}$, $(c^s_{i,\kappa})_{i=1,\ldots,L}$ (resp. λ_κ) is projected on $\{(d_i)_{i=1,\ldots,L} \in [0,1]^L \mid \sum_{i=1}^L d_i = 1\}$ (resp. on $\mathbb{R}_+$) during the updating step. The complete algorithm is detailed in (Eymard and al, 2004) and (Gervais, 2004).

The Newton algorithm presented in this section is also used to solve the nonlinear system resulting from the discretization (15),(7)-(9),(12) with $\mathcal{I}$ set to zero and the flux limiter λ fixed by (12).

4.1.1. *Initialization of the algorithm*

The convergence of the Newton algorithm can be very sensitive to the initialization of the variables. Concerning the sediments thickness variable, taking $h_\kappa = h^n_\kappa + \left(\frac{h^n_\kappa - h^{n-1}_\kappa}{\Delta t^n}\right)\Delta t^{n+1}$ as initial value for the algorithm enables to use the information obtained at the previous time concerning the erosion/sedimentation distribution in the basin. For the flux limiter λ, we can either keep the distribution obtained at the previous time step : $\mathcal{I}_\kappa = \mathcal{I}^n_\kappa$ for all $\kappa \in \mathcal{K}$, or impose $\mathcal{I}_\kappa$ to 0 and λ_κ to one. In the sequel, we shall use the first initialization for λ. Finally, the surface concentration variables are initialized to their previous time step values.

4.1.2. *Jacobian singularities*
The jacobian of the Newton algorithm can be singular due to non-physical situations excluded at convergence. Such cases arise when all the fluxes at the boundary of a cell κ are input or null fluxes and (i) the cell is in erosion, or in addition (ii) the cell is in constrained erosion ($\mathcal{I}_\kappa = 1$). Then, due to the upstream evaluation of the flux limiter and the surface concentrations at the edges between two neighboring cells in the discrete fluxes, the columns of the jacobian corresponding to (i) the variables $c^s_{i,\kappa}$, $i \neq e$, and (ii) in addition the variable λ_κ, vanish. In that cases, the jacobian is modified in such a way that: (i) a sedimentation rate equal e.g. to $1 \times c^s_i$ is added to the conservation equation of the cell κ for each lithology i, and (ii) in addition the sum of the conservation equations in the cell κ over the lithologies is replaced by the equation $\delta\lambda_\kappa = 1 - \lambda_\kappa$.

4.2. Smoothing of the diffusion coefficients

The numerical results presented in section 5.2 point out the lack of robustness of the Newton algorithm, partly due to the jumps of the diffusion coefficients. In order to improve the convergence, a smoothing of the diffusion coefficients on an interval $[-\beta, \beta]$ has been introduced using a linear interpolation in logarithmic scale (see figure 3).

$$k_i(b) = \begin{cases} k_i^c & \text{if } b \leq -\beta, \\ \left(\frac{k_i^m}{k_i^c}\right)^{\frac{b}{2\beta}} (k_i^c\, k_i^m)^{\frac{1}{2}} & \text{if } -\beta < b < \beta, \\ k_i^m & \text{if } b \geq \beta. \end{cases}$$

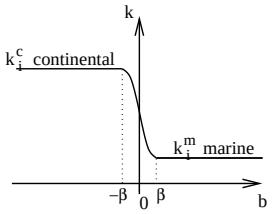

Figure 3. Smoothing of the diffusion coefficients

4.3. Linear iterative solvers with preconditioning

The results discussed in section 5 show that the fully implicit scheme (6)–(10) is the most satisfying according to our objectives. However, at each Newton iteration, a linear system needs to be solved, the size of which increases with the mesh refinement and the number of lithologies. For a large number of unknowns, the solution of this system by a direct sparse solver becomes computationally too expensive and linear iterative solvers must be used to fasten the simulations. The jacobian is non-symmetric and ill-conditioned due to the jumps of the diffusion coefficients and the coupling of mixed parabolic and hyperbolic variables.

A robust, efficient, and scalable solution of the system by an iterative solver requires the construction of a good preconditioner.

In this paragraph, a preconditioning strategy adapted to our system of PDEs is presented. It is based on an approximate decoupling of the variables y and c^s, as well as a proper preconditioning of each block. Its efficiency will be presented in section 5.3 where it is compared to a global preconditioner of ILU type and a sparse direct solver.

In order to simplify the notations, the preconditioning strategy will be presented in the case of vanishing output boundary fluxes which corresponds to all practical test cases. The adaptation to the case of non vanishing output boundary fluxes will be briefly described at each step of the preconditioning strategy, if necessary.

Let $\mathcal{R} = (\mathcal{R}_{i,\kappa})_{i=1,\dots,L,\,\kappa\in\mathcal{K}}$ be the residuals of equations (6) for all $i = 1,\dots,L$ and $\kappa \in \mathcal{K}$ considered as functions of the variable y and the surface concentrations c_i^s, $i = 1,\dots,L$. Then, the Newton iteration amounts to solve the system

$$J \cdot \begin{pmatrix} \delta y \\ \delta c_2^s \\ \vdots \\ \delta c_L^s \end{pmatrix} = \begin{pmatrix} R_1 \\ R_2 \\ \vdots \\ R_L \end{pmatrix} \text{ with } J = \begin{pmatrix} J_{1,y} & -J_{1,1} & \dots & -J_{1,1} \\ J_{2,y} & J_{2,2} & 0 & 0 \\ \vdots & 0 & \ddots & 0 \\ J_{L,y} & 0 & 0 & J_{L,L} \end{pmatrix},$$

where the blocks $J_{i,y}$, $J_{i,i}$, and R_i, $i, j \in \{1,\dots,L\}$, are defined for all κ, $\kappa' \in \mathcal{K}$ by $(J_{i,y})_{\kappa\kappa'} = \partial_{y_{\kappa'}} \mathcal{R}_{i,\kappa}$, $(J_{i,i})_{\kappa\kappa'} = \partial_{c^s_{i,\kappa'}} \mathcal{R}_{i,\kappa}$, and $R_{i,\kappa} = -\mathcal{R}_{i,\kappa}$.

4.3.1. *Preconditioning strategy*

Our preconditioning strategy is based on three main ideas. The first one consists in decoupling the y variable (sediments thickness / flux limiter) from the surface concentrations unknowns in the preconditioner by adapting to our problem the strategy used in (Behie and Vinsome, 1982), (Edwards, 1998) and (Lacroix and al, 2001) for the reservoir simulation, and in (Scheichl and al, 2002) for the sedimentary basin simulation. This decoupling is obtained by linear combinations, for each cell κ, of the conservation equations of the lithologies $i = 1,\dots,L$. It defines, so to speak, an equation for the mixture of lithologies designed to decouple as much as possible the y and c^s variables. The preconditioner for the system is then obtained by a Block Gauss Seidel sweep neglecting the left upper block coupling the y and c^s variables. Note that such a decoupling step preserves the sparsity of the system.

The second idea is to sort the variables by decreasing topographical order in the concentrations blocks $J_{i,i}$ for $i = 2,\dots,L$: thanks to the upwinding of the surface concentrations in the discrete fluxes, we get

lower triangular blocks easily solved by a Gauss Seidel sweep. In the case of non vanishing output boundary fluxes, the Gauss Seidel sweep is to be performed blockwise (of size $L-1$) for the output boundary cells equations.

The third idea is to use an algebraic multigrid V-cycle to precondition the h variable block. Such preconditioner is known to be efficient and scalable for scalar equations of convection diffusion type and to efficiently cope with large jumps of the diffusion coefficients. The full y variable block will be preconditioned using a Block Gauss Seidel approach, with an exact solution of the λ block by a Gauss Seidel sweep for the cells sorted in decreasing topographical order.

4.3.2. *Decoupling*
This step replaces the conservation equation of lithology e on the cell κ by a linear combination of the conservation equations of the lithologies in order to obtain a new equation depending as little as possible on the surface concentrations variables. Let g_κ be the line matrix of dimension L defining this linear combination. The choice of g_κ is crucial for the efficiency of the Block Gauss Seidel preconditioner. In the sequel, the three following definitions of g_κ have been considered.

4.3.2.1. *Sum of the conservation equations* The first idea is to replace the conservation equation of lithology e by the sum of the conservation equations of all the lithologies: $g_\kappa = (\ 1\ \ 1\ \ \ldots\ \ 1\ )$. It leads to a mass term independent of the concentrations and to a flux term at the edge between two neighboring cells κ, κ' equal to $T_{\kappa\kappa'}\lambda_{\kappa\kappa'}[(\psi_i(b_\kappa)-\psi_i(b_{\kappa'}))-(\psi_e(b_\kappa)-\psi_e(b_{\kappa'}))]$ which vanishes for $k_i = k_e$ and is expected to be small for k_i close to k_e.

4.3.2.2. *Weighted sum of the conservation equations* The efficiency of the previous decoupling deteriorates rapidly for increasing ratios between the diffusion coefficients of the lithologies. A better idea is rather to take the sum of the conservation equations of each lithology i weighted by the ratios of the diffusion coefficients $k_1(b_\kappa)/k_i(b_\kappa)$: it leads to a reduction of the dependency of the flux term on the concentrations. For the fully implicit scheme (6)-(10), one obtains

$$\Big[\sum_{i=1}^{L}\frac{k_1(b_\kappa^{n+1})}{k_i(b_\kappa^{n+1})}\frac{\Delta h_{i,\kappa}^{n+1}}{\Delta t^{n+1}}\Big]|\kappa| + \sum_{\kappa'\in\mathcal{K}_\kappa} T_{\kappa\kappa'}\lambda_{\kappa\kappa'}^{n+1}\Big[\sum_{i=1}^{L} c_{i,\kappa\kappa'}^{s,n+1}\frac{k_1(b_\kappa^{n+1})}{k_i(b_\kappa^{n+1})}$$
$$[\psi_i(b_\kappa^{n+1})-\psi_i(b_{\kappa'}^{n+1})]\Big] + \sum_{i=1}^{L}\frac{k_1(b_\kappa^{n+1})}{k_i(b_\kappa^{n+1})}\varphi_{\kappa,e,i}^{n+1} = 0$$

which results in flux terms independent of the concentrations except in the transition zone between marine and continental diffusion. However the mass term still depends on the concentrations in case of sedimentation.

4.3.2.3. *Gaussian elimination* To define a compromise between a decoupling of the mass and flux terms, g_κ is computed in order to cancel the coupling of the variables y and c^s within the cell κ, leading to $g_\kappa = \left(1 \ \frac{(J_{1,1})_{\kappa\kappa}}{(J_{2,2})_{\kappa\kappa}} \ \dots \ \frac{(J_{1,1})_{\kappa\kappa}}{(J_{L,L})_{\kappa\kappa}} \right)$. Note that $(J_{i,i})_{\kappa\kappa}$ is non negative and does not vanish thanks to the correction of the jacobian singularities discussed in section 4.1.2.

In the case of non vanishing output boundary fluxes, the Gauss decoupling is modified for the output boundary cells κ. In such a case, the blocks of the L conservation equations on the cell κ are multiplied by the inverse of the diagonal block of size L within the cell κ.

Let

$$\widetilde{J} = \begin{pmatrix} \widetilde{J}_{1,y} & \widetilde{J}_{1,2} & \dots & \widetilde{J}_{1,L} \\ J_{2,y} & J_{2,2} & 0 & 0 \\ \vdots & 0 & \ddots & 0 \\ J_{L,y} & 0 & 0 & J_{L,L} \end{pmatrix},$$

denote the jacobian after the decoupling step, then the Block Gauss Seidel preconditioner of $\widetilde{J}$ writes

$$C^{-1} = \begin{pmatrix} C_{1,y} & 0 & \dots & 0 \\ J_{2,y} & J_{2,2} & 0 & 0 \\ \vdots & 0 & \ddots & 0 \\ J_{L,y} & 0 & 0 & J_{L,L} \end{pmatrix}^{-1},$$

where the choice of the preconditioner $C_{1,y}^{-1}$ is discussed in the next subsection.

4.3.3. *Block preconditioner* $C_{1,y}^{-1}$

The choice of the preconditioner $C_{1,y}^{-1}$ of the block $\widetilde{J}_{1,y}$ which concentrates the stiffness of the linear system is crucial for the efficiency of the iterative solver. In the following, we will compare an exact inversion $C_{1,y}^{-1} = \widetilde{J}_{1,y}^{-1}$ of the linear system using a sparse direct solver, an incomplete factorization ILU(0), and an algebraic multigrid preconditioner (AMG).

As opposed to the first two choices, AMG preconditioners are known to achieve scalability for convection diffusion operator with large jumps of the diffusion coefficients. However they cannot apply directly to the

system $\widetilde{J}_{1,y}^{-1}$ coupling the h and λ variables of mixed parabolic and hyperbolic types. In the numerical test the AMG V-cycles applied to the block $\widetilde{J}_{1,y}$ does not converge due to the non diagonal dominance of the lines for which $\mathcal{I}_\kappa = 1$ (i.e. $y_\kappa = \lambda_\kappa$). This is why the AMG preconditioner will only be applied to the h variable. Let us consider the partition $\mathcal{K}_h = \{\kappa \in \mathcal{K} \,/\, \mathcal{I}_\kappa = 0\}$, $\mathcal{K}_\lambda = \{\kappa \in \mathcal{K} \,/\, \mathcal{I}_\kappa = 1\}$ of the set of cells $\mathcal{K}$, and let

$$\begin{pmatrix} \widetilde{J}_{h,h} & \widetilde{J}_{h,\lambda} \\ \widetilde{J}_{\lambda,h} & \widetilde{J}_{\lambda,\lambda} \end{pmatrix} \tag{17}$$

denote the corresponding block representation of the system $\widetilde{J}_{1,y}$. The coupling of the h and λ variables only arises at the interface between constrained and unconstrained cells. Hence the block $\widetilde{J}_{h,\lambda}$ will be neglected in the preconditioner, leading to the following Block Gauss Seidel preconditioner of $\widetilde{J}_{1,y}$

$$C_{1,y}^{-1} = \begin{pmatrix} C_{h,h} & 0 \\ \widetilde{J}_{\lambda,h} & \widetilde{J}_{\lambda,\lambda} \end{pmatrix}^{-1}, \tag{18}$$

for which the inversion of the $\widetilde{J}_{\lambda,\lambda}$ system is achieved by a Gauss Seidel sweep for the cells sorted in decreasing topographical order, and the preconditioner $C_{h,h}^{-1}$ is one V-cycle of an AMG solver. More precisely, we shall use in the numerical tests the AMG code `AMG1R5` (release 1.5, 1990) (Ruge and Stüben, 1986).

5. Numerical results

5.1. Test cases

The code computing the solution of the fully implicit scheme (6)–(10) and the semi-implicit scheme (15),(7)-(9),(12) has been applied to real data sets. In this article, we will consider the two following cases.

5.1.1. *Paris basin test case*

The first test case uses input data corresponding to the Paris basin (France) for base level, sea level and sediment supply, defined using (Mégien and al, 1980), (Guillocheau, 2000) and (Gonçalvès, 2002). The simulated zone is 500 km long by 400 km large, filled with two lithologies (sand and shale). The simulation is performed over 40 My. The initial concentrations are $c_1^0 = c_2^0 = 0.5$, the maximum erosion rate is taken equal to 3 m/My and the diffusion coefficients to $k_1^c = 10^5\, m^2/y$, $k_1^m = 10^4\, m^2/y$, $k_2^c = 2.10^6\, m^2/y$ and $k_2^m = 4.10^4\, m^2/y$.

Figure 4 exhibits the initial and final topographies in the basin as well as the final sand concentration.

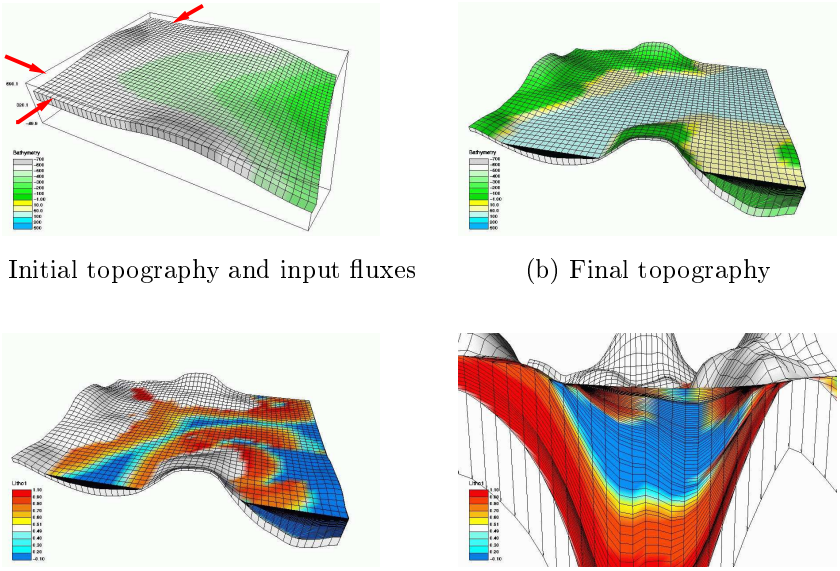

(a) Initial topography and input fluxes (b) Final topography

(c) Final sand concentration (d) Final sand concentration (cut)

Figure 4. Paris test case : initial and final topographies, and final sand concentration in the basin.

5.1.2. *Rift basin test case*

The basin domain Ω is a square of length 180 km, with no eustatics variations and no base level displacement. Figure 5 exhibits the initial topography as well as the final topography after a simulation time span of 3 My. The Rift basin has five sediments input fluxes at its boundary, it is filled with two lithologies (sand and shale) of diffusion coefficients $k_{1,c} = k_{2,c} = 7570$ m^2/y, $k_{1,m} = 4425$ m^2/y, $k_{2,m} = 44250$ m^2/y. The maximum erosion rate is fixed to $E = 100$ m/My, and the initial basin concentrations are $c_1^0 = c_2^0 = 0.5$.

For both test cases, the mesh is a uniform Cartesian grid of size Δx, and the maximum time step is denoted by Δt. The time step is restarted with a twice smaller value in case of non convergence of the Newton algorithm after 35 iterations, with a convergence stopping criterion fixed to 10^{-6} for the relative l^2 norm of the conservation equations residuals. On the contrary, the next time step is increased by a factor 1.2 in the limit of the maximum time step Δt. For the semi-implicit scheme, the simulation is initialized with a time step equal to $\Delta t/10$

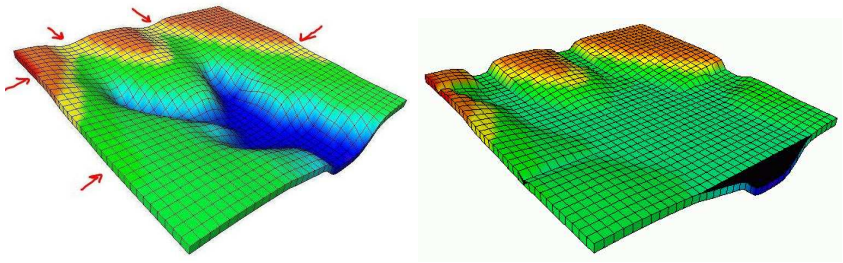

Figure 5. Initial (left) and final (right) topographies of the Rift basin.

while it is started with the time step Δt for the fully implicit scheme.

In the following tests, the Block Gauss Seidel preconditioners of $\widetilde{J}$ will be denoted by BGSLU for $C_{1,y}^{-1} = \widetilde{J}_{1,y}^{-1}$, BGSILU for $C_{1,y}^{-1}$ given by the ILU(0) incomplete factorization of $\widetilde{J}_{1,y}$, and BGSAMG for $C_{1,y}^{-1}$ defined by (18).

These block preconditioners will be compared to a direct sparse solver from the `PETSc` library of the Argonne National Laboratory, IL (Balay and al, 2001), denoted by DIRECT, and to the ILU(0) incomplete factorization of $\widetilde{J}$ denoted by ILU. They will also be compared to the semi-implicit scheme with the BGSAMG solver, denoted by BGSAMG-SI.

The stopping criterion for the iterative solvers is fixed to 10^{-6} for the relative residual in l^2 norm. Inexact Newton approaches have also been tested with no improvement in terms of CPU times, hence they will not be presented in the following.

The iterative solver is GMRES (Saad and Schultz, 1986) with a maximum Krylov subspace dimension fixed at 100. All the tests are performed on a PC DELL M60 1.3 Mhz with LINUX operating system.

5.2. Newton algorithm

Table I exhibits for the Paris test case, the fully implicit scheme and the semi-implicit scheme, the performance of the Newton algorithm for different values of the mesh size Δx and the smoothing parameter β. The lack of robustness of the Newton algorithm for the fully implicit scheme is due to the combination of severe nonlinearities induced by the transitions between the sediments transport laws in the basin : unconstrained diffusion ($\lambda = 1$) / constrained erosion ($\partial_t h = -E$), sedimentation / erosion, and continental diffusion / marine diffusion.

The smoothing of the diffusion coefficients considerably improves the convergence for fine grids. This smoothing has to be determined for each test case to obtain a good compromise between an improvement

of the Newton convergence and a physically admissible basin profile at the shoreline. To achieve this, β is chosen adaptatively proportional to the maximum slope at the shoreline

$$\beta = \gamma \text{ diameter}(\Omega) \max_{\kappa|\kappa'\in\Sigma_{int},\ b_\kappa b_{\kappa'}<0} \frac{|b_\kappa - b_{\kappa'}|}{d(\kappa,\kappa')},$$

computed at the previous time step.

The results of table I exhibit a much better and scalable convergence of the Newton algorithm for the semi-implicit scheme, which confirms the crucial role of the nonlinearity induced by the unilaterality constraint on the lack of robustness of the Newton algorithm for the fully implicit scheme.

However, the solution of the semi-implicit scheme is not accurate at the transition between a constrained continental erosion and an unconstrained marine erosion due to the computation of the product $\lambda^n k_i(b^{n+1})$ with λ and k_i taken at different time steps. This results in oscillations of the topography at the shoreline of amplitude decreasing with the time step. To improve the solution, one could compute the flux limiter λ^{n+1} using the sea and base levels at time t^{n+2} rather than t^{n+1} : the solution is more accurate but the Newton convergence deteriorates. A better solution in term of Newton convergence is to take both the flux limiter λ and the diffusion coefficients $k_i(b)$ explicit in time, but in that case, an accurate solution requires very small time steps due to the large jumps of the marine and continental diffusion coefficients.

Table I. Total number of Newton iterations and average number of Newton iterations per time step for different values of the smoothing parameter β, the fully implicit and the semi-implicit schemes, with the BGSAMG solver, $e = 2$, and the Gauss decoupling. Paris basin test case with $\Delta t = 0.1$ My.

scheme	Δx (km)	β= 5 m	β= 10 m	β= 20 m
fully implicit	10	2410/5.9	2150/5.3	2030/5.1
	5	3860/9.1	3320/8.1	3040/7.6
	2.5	8640/17.6	7360/16.1	5910/13.9
semi-implicit	10	1467/3.6	1346/3.3	1308/3.2
	5	1532/3.75	1423/3.5	1386/3.4
	2.5	1595/3.9	1487/3.6	1447/3.5

5.3. Linear iterative solvers

5.3.1. *Decoupling, choice of the lithology e, and $J_{i,i}$ preconditioner*
Table II exhibits, on the Rift basin test case, the influence of each of the three decoupling methods of subsection 4.3.2, as well as the influence of the choice of the eliminated lithology e, on the performance of the linear solver BGSLU. We conclude that the Gauss decoupling method is the most efficient, and that $e = 2$ is the best choice which corresponds to the most diffusive lithology.

Table III compares four block preconditioning strategies with in all cases an exact solve of the $\widetilde{J}_{1,y}$ block. The first one (Block Gauss Seidel) is defined by (4.3.2.3), the second one (Point Gauss Seidel) uses a Gauss Seidel sweep preconditioning in the cell original order rather than an exact solve of the blocks $J_{i,i}$ in (4.3.2.3). The third one (Block Jacobi) uses a Block Jacobi preconditioner ($J_{i,y}$ set to zero in (4.3.2.3)), and the fourth one (Point Jacobi) uses in addition a diagonal preconditioning of the blocks $J_{i,i}$ rather than an exact solve.

The results on the Rift basin test case illustrate that it is essential to solve accurately the concentration blocks $J_{i,i}$, $i = 2, \ldots, L$, and to use a Block Gauss Seidel rather than a Block Jacobi preconditioner, to obtain a good convergence of the iterative solver.

The same conclusions hold for the Paris basin test case, and for all the numerical experiments that have been carried out on various test cases. Hence, the following experiments will be performed with e chosen as the most diffusive lithology (well defined since in all cases $k_i^m, i = 1, \ldots, L$, and $k_i^c, i = 1, \ldots, L$ have the same ordering), with the Gauss decoupling, and the Block Gauss Seidel preconditioner (4.3.2.3).

Table II. Influence of the decoupling g_κ and the choice of e on the number of GMRES iterations and on the simulation time with the BGSLU preconditioner. Rift basin test case with $\Delta x = 2.5$ km, $\Delta t = 0.03$ My, $\beta = 10$ m.

Decoupl. 4.3.2.1 $e = 2$	Decoupl. 4.3.2.2 $e = 2$	Decoupl. 4.3.2.3 $e = 2$	Decoupl. 4.3.2.3 $e = 1$
21.9 it.	18.8 it.	9.3 it.	17.6 it.
177 s	160 s	111 s	154 s

Table III. Number of GMRES iterations and simulation time for the BGS preconditioner with $e = 2$, the Gauss decoupling, $C_{1,y}^{-1} = \widetilde{J}_{1,y}^{-1}$, and different choices of the preconditioning of the other blocks. Rift basin test case with $\Delta x = 2.5$ km, $\Delta t = 0.03$ My, $\beta = 10$ m.

Point Jacobi	Point Gauss Seidel	Block Jacobi	Block Gauss Seidel
84 it.	53 it.	19.5 it.	9.3 it.
571 s	383 s	156 s	111 s

5.3.2. *Comparison and scalability of the preconditioners*
Tables IV, V, and figures 6, 7 compare the efficiency and scalability of the various solvers for the Paris and Rift basins test cases. We conclude that it is essential to have a very good preconditioning of the $\widetilde{J}_{1,y}$ block which is very ill conditioned due to its parabolic nature and the large jumps of the diffusion coefficients. The ILU(0) incomplete factorization preconditioner is not at all robust and scalable neither on the full system nor on the $\widetilde{J}_{1,y}$ block. For the Paris basin test case, it is even much worse than the direct solver on the fine grid.

In terms of GMRES iterations, the BGSLU preconditioner is the most efficient and exhibits a very good scalability. However, especially for fine grids, the BGSAMG preconditioner is clearly more efficient and scalable in CPU time despite a small loss in terms of GMRES iterations. All together this is the best preconditioner for the fully implicit scheme.

The BGSAMG solver performs even better for the semi-implicit scheme (BGSAMG-IS), due to the fact that the AMG solver applies in that case to the full block $\widetilde{J}_{1,y} = \widetilde{J}_{h,h}$.

Table VI illustrates the very good scalability of the preconditioners BGSLU and BGSAMG for the Rift test case, with respect to the ratios of the diffusion coefficients $r_{2,1} = \frac{k_{2,c}}{k_{1,c}} = \frac{k_{2,m}}{k_{1,m}}$, as well as $r_{m,c} = \frac{k_{1,m}}{k_{1,c}} = \frac{k_{2,m}}{k_{2,c}}$. These results also confirm that the BGSAMG solver is, in most cases, the most efficient solver in terms of CPU time.

Table IV. Number of GMRES iterations per Newton/total simulation time in seconds, for the various solvers. Paris basin test case with $\beta = 20$ m, and $\Delta t = 0.1$ My.

Δx (km)	Direct	ILU	BGSILU	BGSLU	BGSAMG	BGSAMG-SI
10	1/132	31/124	42/139	11.6/83	15.4/62	12/52
5	1/1133	66/1700	83/2250	13.5/790	20/530	12.6/259
2.5	1/18450	142/51800	199/85020	16/9110	27/5925	13.2/1226

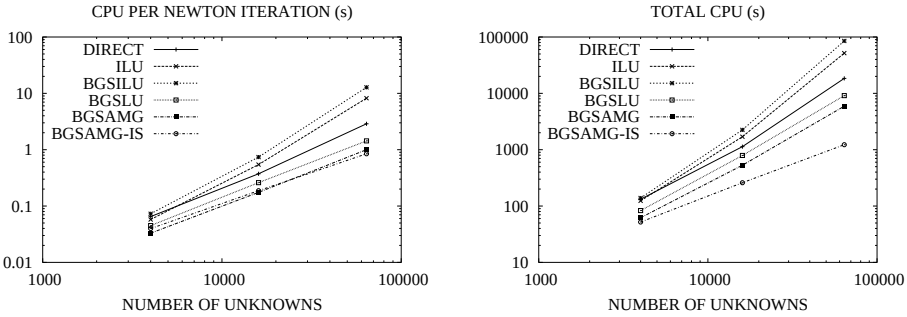

Figure 6. CPU time per Newton (left), and CPU time of the simulation (right). Paris basin test case with $\beta = 20$ m, and $\Delta t = 0.1$ My.

Table V. Number of GMRES iterations per Newton/total simulation time in seconds, for the various solvers. Rift basin test case with $\beta = 10$ m, and $\Delta t = 0.03$ My.

Δx (km)	Direct	ILU	BGSILU	BGSLU	BGSAMG	BGSAMG-SI
5	1/25	28/23	32/20.5	9.1/14	12.3/14.4	11/12
2.5	1/190	55/230	57/237	9.3/111	14.2/98	12/65
1.25	1/5405	105/3840	103/3630	9.23/1770	16.8/750	12.5/415

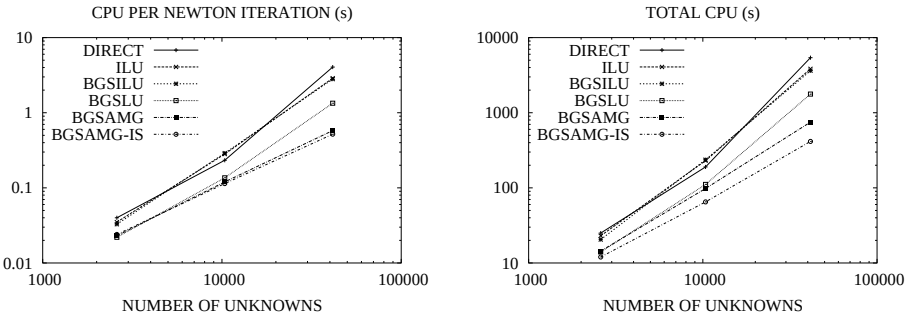

Figure 7. CPU time per Newton (left), and CPU time of the simulation (right) for the various solvers. Rift basin test case with $\beta = 10$ m, and $\Delta t = 0.03$ My.

Table VI. Number of GMRES iterations per Newton and total simulation time in seconds for the BGSLU and BGSAMG solvers and the following values of the diffusion coefficients: left: $k_{1,c} = 7570$ m^2/y, $k_{1,m} = 4425$ m^2/y, and $k_{2,c} = r_{2,1}\ k_{1,c}$, $k_{2,m} = r_{2,1}\ k_{1,m}$, and right: $k_{1,c} = 7570$ m^2/y, $k_{2,c} = 75700$ m^2/y, and $k_{1,m} = r_{m,c}\ k_{1,c}$, $k_{2,m} = r_{m,c}\ k_{2,c}$. Rift basin test case with $\Delta x = 2.5$ km, $\Delta t = 0.03$ Ma, and $\beta = 10$ m.

$r_{2,1}$	BGSLU	BGSAMG	$r_{m,c}$	BGSLU	BGSAMG
100	12.5/157	20.4/151	100	12.6/403	20.4/337
10	9.2/112	14.2/100	10	10.9/179	15.9/130
1	1/49	8.8/53	1	9.3/108	14.4/95
0.1	9.5/81	11.6/67	0.1	9.0/85	12.4/74
0.01	12.8/87	13.8/69	0.01	10.8/88	13.3/77

6. Conclusion

This article has presented numerical algorithms to simulate a multilithology stratigraphic model used in oil exploration for the infill of sedimentary basins at large scales in space and time, governed by the interaction between tectonics displacements, eustatics variations, sediments supply and sediments transport laws. These algorithms, ranging from time and space discretizations, nonlinear and linear preconditioned iterative solvers, result in a simulation code which preserves the physical bounds of the model, captures accurately the main nonlinear transitions between the different transport laws within the basin, and has good scalability properties with respect to the size of the mesh and the jumps of the diffusion coefficients.

Acknowledgements

The authors would like to thank Didier Granjeon from the Geology department of the Institut Français du Pétrole for numerous discussions on the model and for providing the real basin test cases, as well as Sylvie Wolf from the applied mathematics department of IFP, Professors Thierry Gallouët from the Université de Provence and Robert Eymard from the Université de Marne la Vallée for fruitful discussions and comments during the elaboration of this work.

References

J. C. Rivenaes, Application of a dual-lithology, depth-dependent diffusion equation in stratigraphic simulation, *Basin Research*, 9, 91-105, 1992.

D. Granjeon, *Modélisation Stratigraphique Déterministe : Conception et Application d'un Modèle Diffusif 3D Multilithologique*, PhD Thesis, Geosciences, Université de Rennes, France, 1997.

D. Granjeon and P. Joseph, Concepts and applications of a 3D multiple lithology, diffusive model in stratigraphic modelling, in *Numerical Experiments in Stratigraphy*, J.W. Harbaugh and al., editors, SEPM Sp. Publ., 62, 1999.

R. Eymard, T. Gallouët, D. Granjeon, R. Masson and Q.H. Tran, Multi-lithology stratigraphic model under maximum erosion rate constraint, *Int. Journal of Num. Methods in Eng.*, 60:527-548, 2004.

G. Behie and P. Vinsome, Block iterative methods for fully implicit reservoir simulation, *SPE Journal*, 658-668, 1982.

H. C. Edwards, A parallel multilevel preconditioned GMRES solver for multiphase flow models in the Implicit Parallel Accurate Reservoir Simulator (IPARS), *TICAM Report 98-04*, The University of Texas at Austin, 1998.

S. Lacroix, Y. V. Vassilevski and M. F. Wheeler. Decoupling preconditioners in the Implicit Parallel Accurate Reservoir Simulator (IPARS). *Numer. Linear Algebra Appl.*, 8:537-549, 2001.

R. Scheichl, R. Masson and J. Wendebourg, Decoupling and block preconditioning for sedimentary basin simulations, *Computational Geosciences*, 7, 295-318, 2003.

R. S Anderson and N. F Humphrey, Interaction of Weathering and Transport Processes in the Evolution of Arid Landscapes, In T. A. Cross, ed., *Quantitative Dynamics Stratigraphy*, Prentice Hall, 349-361, 1989.

R. Eymard and T. Gallouët, Analytical and numerical study of a model of erosion and sedimentation, *submitted to SIAM J. Num. Anal.*, 2004.

E. Eymard, T. Gallouët, V. Gervais and R. Masson, Convergence of a numerical scheme for stratigraphic modeling, *SIAM J. Num. Anal.*, (accepted for publication), 2004.

V. Gervais and R. Masson, Mathematical and numerical analysis of a stratigraphic model, *M2AN*, 38, 585-611, 2004.

V. Gervais, *Etude et simulation d'un modèle stratigraphique multi-lithologique sous contrainte de taux d'érosion maximal*, PhD thesis, Université de Provence, France, 218 p., 2004.

E. Eymard, T. Gallouët and R. Herbin, *The finite volume method*, in P. Ciarlet and J. Lions, eds., Handbook of Numerical Analysis, Elsevier, 7:715-1022, 2000.

O. Kavian. Introduction à la théorie des points critiques et applications aux problèmes elliptiques. In Mathématiques et Applications 13, Springer-Verlag, 97-115, 1993.

J.G. Heywood and R. Rannacker. Finite Element approximation of the nonstationary Navier-Stokes problem. Part IV : error analysis for second-order time discretization. *SIAM J. Num. Anal.*, 27, 353-384, 1990.

J.W. Ruge and K. Stüben, Algebraic Multigrid (AMG), in: *Multigrid Methods*, ed. S.F. McCormick, Frontiers in Applied Mathematics, Vol. 5 (SIAM Philadelphia, 1986).

C. Mégien. Synthèse organique du Bassin de Paris. Mémoire BRGM 101, 1980.

F. Guillocheau, Meso-Cenozoic geodynamic evolution of the Paris basin : a 3D stratigraphic constraints, *Geodinamica Acta*, 13, 189-246, 2000.

J. Gonçalvès, *Modélisation 3D de l'évolution géologique du Bassin de Paris : implications diagénétiques et hydrogéologiques*, PhD Thesis, Université de Paris VI, France, 302 p., 2004.

S. Balay, W. Gropp, L.C. McInnes, and B. Smith, *PETSc Users Manual*, Technical Report ANL-95/11 – Revision 2.1.0, Argonne National Laboratory, IL (2001).

Y. Saad and M.H. Schultz, GMRES: a generalized minimal residual algorithm for solving nonsymmetric linear systems, *SIAM J. on Scientific and Statistical Computing*, Vol. 7, 3, 856-869, 1986.